Journal of Solid State Chemistry 278 (2019) 120927

Contents lists available at ScienceDirect

Journal of Solid State Chemistry

journal homepage: www.elsevier.com/locate/jssc

# Two $Pb^{II}$-based coordination polymers based on 5-aminonicotinic acid and 5-hydroxynicotinic acid for Knoevenagel condensation reaction and luminescent sensor

Xiuling Zhang [a,*], Ranhui Zhang [a,b], Yaoqiang Jin [a,b], Tingting Li [a,c]

[a] College of Chemistry and Chemical Engineering, Dezhou University, Dezhou, 253023, PR China
[b] College of Chemical Engineering, Qingdao University of Science and Technology, Qingdao, 266000, PR China
[c] College of Chemical Engineering, Xi'an Polytechnic University, Xi'an, 710048, PR China

ARTICLE INFO

*Keywords:*
$Pb^{II}$-Based coordination compound
Luminescent sensor
Catalysis
$Fe^{3+}$

ABSTRACT

Two new $Pb^{II}$-based coordination polymers based on 5-aminonicotinic acid (namely HL–$NH_2$) and 5-hydroxynicotinic acid (namely HL–OH) are both successfully synthesized under solvothermal synthesis conditions. $PbCl_2$ and HL-$NH_2$ can generate a 3D network with the formula of $\{[Pb_3(L\text{-}NH_2)_2Cl_5]\cdot(H_2O)\}_n$ (complex **1**). The –$NH_2$ functional group is replaced by –OH on the organic linker to further coordinate with $Pb^{II}$ to fabricate another 3D framework of $[Pb_2(L\text{–}O)Cl_2]_n$ (complex **2**). Interestingly, various and fanatics structures can be tuned and regulated by different functional substituent groups. Furthermore, complex **1** can be applied as a high-efficient heterogeneous catalysis for Knoevenagel condensation reaction. Meanwhile, complex **2** is an excellent potential luminescent sensor for $Fe^{3+}$.

## 1. Introduction

In these decades, a good deal of efforts have been directly focused on tuning and designing coordination compounds, also called metal–organic frameworks (MOFs) [1–4], which is not only due to their various networks and widely potential applications in lots of fields, including catalysis [5–8], optical device [9–11], fluorescent sensor [12–15], enzyme carriation [16–18], and gas adsorption or separation [19–23]. Nevertheless, it is a significant challenge to really understand structures and properties relationships at the present investigate stage. In the view of crystal engineering, organic linkers with different coordinated sites and structures are considered as the most important factor to construct coordination compounds [24–28]. On the other hand, chemical and physical factors all can affect the final structures, such as solvent, pressure, template, temperature, pH value and so on [29–35]. –$NH_2$ and –OH functional groups are always introduced in linkers to affect the structures and properties, because they have different coordination abilities and acid-base property. Different structures and functional groups can directly affect their physicochemical performances. The displacement result of hydrogen atom by –$NH_2$ and –OH functional groups will have remarkable influences in many aspects, especially catalytic and gas sorption [36–40]. In the other previous reports, –$NH_2$ group can be applied as a good candidate to catalyse Knoevenagel condensation reaction [41–44]. Meanwhile, MOFs based on 5-hydroxynicotinic acid can be used as luminescent sensors to detect hazardous substances. Herein, a systematic study is investigated and reported to design and synthesize two three-dimensional (3D) $Pb^{II}$ MOFs, including complex **1** based on 5-aminonicotinic acid (namely HL–$NH_2$) and complex **2** based on 5-hydroxynicotinic acid (namely HL–OH). More importantly, complex **1** can be used a heterogeneous catalyst for Knoevenagel condensation reaction, meanwhile complex **2** can be considered as a luminescent sensor for $Fe^{3+}$ with good recyclability.

## 2. Experimental

### 2.1. Materials and general methods

All chemicals and reagents were purchased from reagent companies and used directly in this work. All powder X-ray diffraction (PXRD) were achieved from a Riguku D8 ADVANCE with Cu-Kα (λ = 1.5418 Å) from 5° to 50° of 2θ value. Elemental analyses (C, H, and N) were analysed on a VarioEL cube analyzer. Thermogravimetric analyses (TGA) data were acquired on a TGA Q500 machine in a $N_2$ condition with 10 °C $min^{-1}$ heating rate. The catalytic data were calculated by GC method on a

* Corresponding author.
*E-mail address:* xlzhang99@126.com (X. Zhang).

https://doi.org/10.1016/j.jssc.2019.120927
Received 28 July 2019; Received in revised form 18 August 2019; Accepted 22 August 2019
Available online 26 August 2019

**Table 1**
Crystal data and structure refinement for **1** and **2**.

| Compound | 1 | 2 |
|---|---|---|
| Empirical formula | $C_{12}H_6O_5N_4Cl_5Pb_3$ | $C_6H_3O_3NCl_2Pb_2$ |
| Formula weight | 1085.12 | 622.37 |
| Crystal system | monoclinic | orthorhombic |
| Space group | $P2_1/n$ | $P2_12_12_1$ |
| $a$ (Å) | 13.9215 (16) | 8.0846 (17) |
| $b$ (Å) | 8.2851 (9) | 8.8824 (18) |
| $c$ (Å) | 19.683 (2) | 13.903 (3) |
| $\alpha$ (°) | 90 | 90 |
| $\beta$ (°) | 107.424 (2) | 90 |
| $\gamma$ (°) | 90 | 90 |
| $V$ (Å$^3$) | 2166.1 (4) | 998.4 (4) |
| $Z$ | 4 | 4 |
| $\rho$ (calc g cm$^{-3}$) | 3.327 | 4.140 |
| $\mu$ (mm$^{-1}$) | 23.915 | 34.192 |
| $N$ref | 3820 | 1759 |
| $R$ (int) | 0.0666 | 0.0500 |
| Goodness-of-fit on F [2] | 1.029 | 0.981 |
| $R_1$, w$R_2$ [I > 2σ(I)] | 0.0343, 0.0630 | 0.0239, 0.0543 |
| $R_1$, w$R_2$ (all data) | 0.0487, 0.0681 | 0.0247, 0.0547 |

TRACE 1300 instrument. Luminescent spectra were obtained on a Cary Eclipse fluorescence spectrophotometer. UV–Vis absorption spectra were performed on a UV-1200UV-1100.

### 2.2. Syntheses of complex **1** and **2**

#### 2.2.1. Preparation of $\{[Pb_3(L\text{-}NH_2)_2Cl_5]\cdot(H_2O)\}_n$ (complex **1**)

$PbCl_2$ (20 mg) and HL-$NH_2$ (8 mg) were both dissolved in a mixture solution of $CH_3CN$ (2.5 mL) and $H_2O$ (1.5 mL), which was heated at 100 °C for 5 days in a Telfon-lined stainless steel vessel under an autogenous pressure. After the reaction vessel was gradually cooled down to room temperature, light yellow single crystals with well shape of complex **1** were collected and dried in air with a 59% yield based on HL-$NH_2$. Anal. Calcd for $C_{12}H_8O_5N_4Cl_5Pb_3$: C, 13.3; H, 0.7; N, 5.2%. Found: C, 13.4; H, 0.6; N, 5.2%.

#### 2.2.2. Syntheses of $[Pb_2(L\text{–}O)Cl_2]_n$ (complex **2**)

A mixture of HL–OH (8 mg), $PbCl_2$ (25 mg) was putted in $CH_3CN$ (2.5 mL) and $H_2O$ (1.5 mL), which was further added 0.1 mL of NaOH (0.1 M). The resultant mixture was heated at 100 °C for 4 days in a sealed Telfon-lined stainless steel vessel. After it was slowly cooled down to room temperature, yellow block crystals with good quality can be

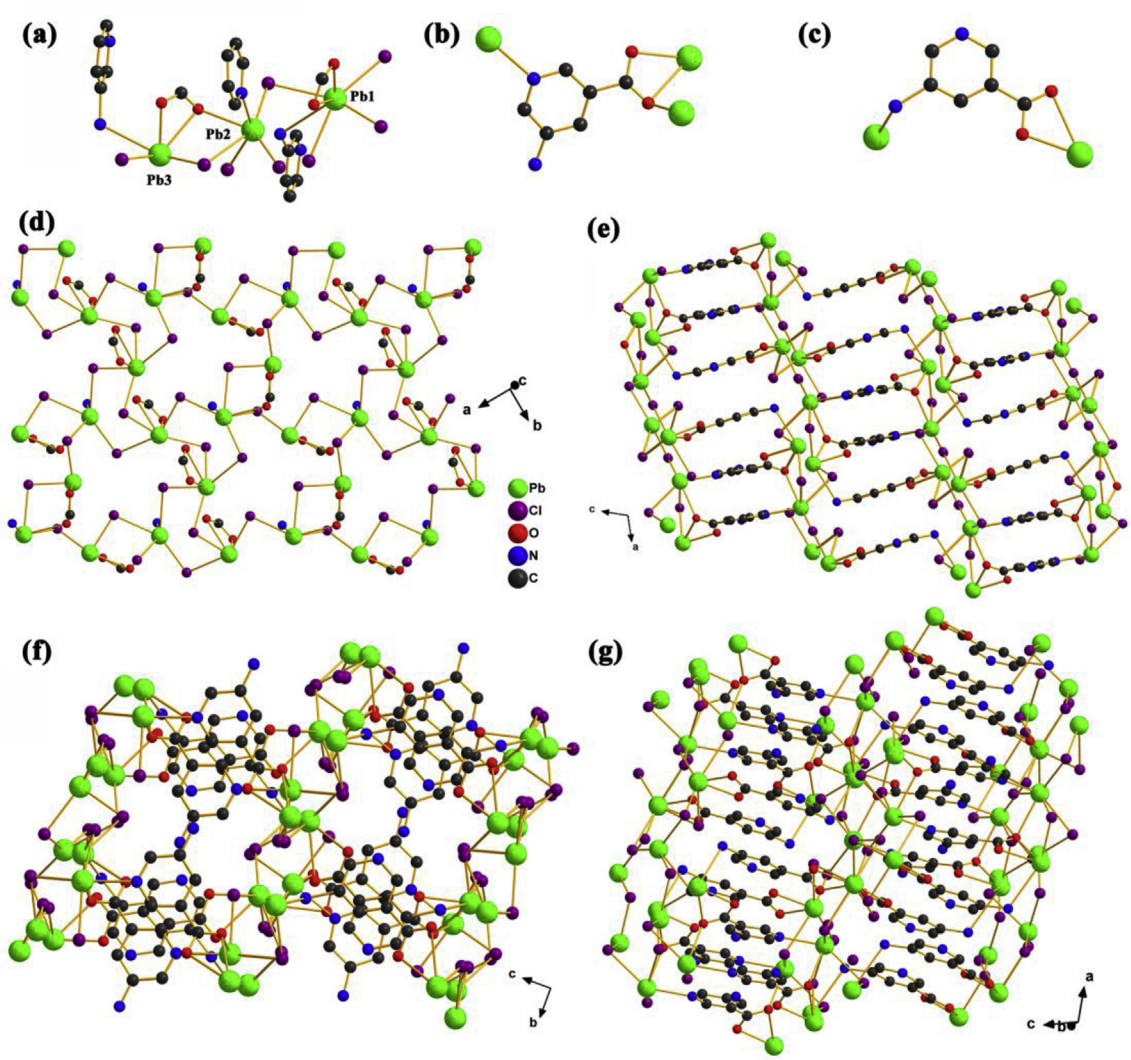


**Fig. 1.** (a) Coordination environment of $Pb^{II}$; (b and c) coordination modes of L–$NH_2^-$ ligand; (d) viewing of the 2D layer; and (e–g) 3D structures in different axises (all hydrogen atoms are omitted for clarity, and C, black; O, red; N, blue; Cl, purple; Pb, green). (For interpretation of the references to colour in this figure legend, the reader is referred to the Web version of this article.)

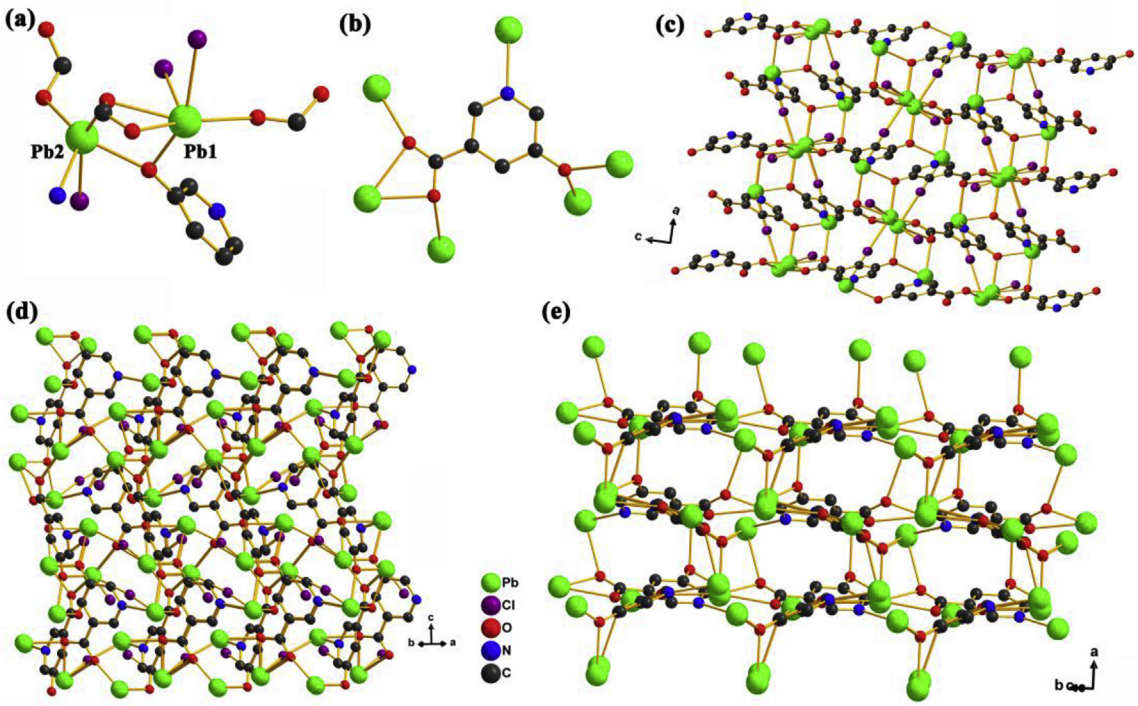


**Fig. 2.** (a) Coordination environment of $Pb^{II}$ cation in complex **2**; (b) coordination mode of L–$O^{2-}$ ligand; and (c–e) viewing of 3D structure along different axises (all hydrogen atoms are removed for clarity, and C, black; O, red; N, blue; Cl, purple; Pb, green). (For interpretation of the references to colour in this figure legend, the reader is referred to the Web version of this article.)

achieved in a 63% yield based on HL-OH. Anal. Calcd for $C_6H_3O_3NCl_2Pb_2$: C, 11.6; H, 0.5; N, 2.3%. Found: C, 11.3; H, 0.4; N, 2.2%.

### 2.3. X-ray structure determination and structure refinement

Single crystal data of **1** and **2** were both measured on a Bruker SMART CCD diffractometer with Mo $K_\alpha$ radiation ($\lambda = 0.71073$ Å). Crystal frameworks can be located precisely by the direct approach with *SHELXT 6*, which was further refined by using the full-matrix least-squares technique with *SHELXL-2015* [45,46] and *OLEX2* software [47]. In addition, all non-hydrogen atoms were confirmed by using anisotropic displacement parameters. Table 1 summarizes in all crystal data.

### 2.4. Typical catalysis procedure

Complex **1** was dried in air and then soaked in toluene for 1 day prior the catalytic reaction. In a typical procedure, substrate (1 mmol) and malononitrile (1.1 mmol) were both mixed in a round-bottom flask with toluene (5 mL). The reaction mixture was heated and kept at 85 °C. Complex **1** (~100 mg) was added into the above reaction system and slowly stirred under this condition. The final catalytic yields can be calculated by the GC method.

### 2.5. Recyclable catalysis experiment

The recyclability of **1** can be easily regenerated by centrifugation and washing by fresh toluene for several times. The re-collected samples were further reused as a catalyst for the continuous catalytic reaction.

### 2.6. Luminescent sensing experiments

As-synthesized **2** was ground several minutes in a mortar to significantly reduce the size before all sensing trials. Ground **2** was selected and studied for luminescent detectable experiments. Ground **2** (3.0 mg) firstly well dispersed in 3.0 mL N, *N*-dimethylformamide (DMF) for next experiments. All emission intensities of the above dispersions were performed and collected in different DMF solutions of $M(NO_3)_x$ ($M^{x+} = Li^+$, $Na^+$, $K^+$, $Ag^+$, $Zn^{2+}$, $Mn^{2+}$, $Mg^{2+}$, $Cd^{2+}$, $Ca^{2+}$, $Co^{2+}$, $Cu^{2+}$, $Ni^{2+}$, $Fe^{2+}$, and $Fe^{3+}$, $5.0 \times 10^{-4}$ mol $L^{-1}$) after immersing 2 min.

### 2.7. The typical luminescence titration for complex 2

Powder crystal **2** was carefully putted in 3 mL DMF to generate 1.0 mg $mL^{-1}$ suspension in a quartz cell, which was used for all sensing titration trials. The titration experiments were measured by slowly introducing $Fe^{3+}$ and further repeated at least three times.

## 3. Results and discussion

### 3.1. Structural description for complex 1

Single-crystal X-ray diffraction data obviously exhibit that complex **1** crystallizes in monoclinic crystal system and $P2_1/n$ space group. As seen in Fig. S1, the asymmetric unit has three $Pb^{II}$ atoms, five $Cl^-$ atoms, two crystallographically independent L–$NH_2^-$ ligands and a free O atom. As shown in Fig. 1a, Pb1 atom is linked with seven atoms, including two O atoms from a cheating carboxylate group, four $Cl^-$ atoms, and one N atom from –$NH_2$, respectively. Pb2 atom is connected with six atoms, including an oxygen atom from a cheating carboxylate group, four $Cl^-$ atoms, and one N atom from –$NH_2$, respectively. Pb3 is surrounded by five coordinated atoms from two $Cl^-$ atoms, two atoms from a cheating carboxylate group, and one N atom from –$NH_2$, respectively. The deprotonated L–$NH_2^-$ ligands adopt two different coordination modes $\mu_3$-$\eta^2$: $\eta^1$: $\eta^1$ and $\mu_2$-$\eta^1$: $\eta^1$: $\eta^1$, which are on a scale of one to one in the structure (Fig. 1b and c). As illustrated in Fig. 1d, complex **1** has a two dimensional (2D) layer by using bridging $Cl^-$. Furthermore, there different layers can be further connected by –$COO^-$ groups of bridging linkers to construct a 3D network (Fig. 1e–g).

Single crystal data of as-synthesized complex **2** shows that it is the orthorhombic crystal system with the $P2_12_12_1$ space group. In its

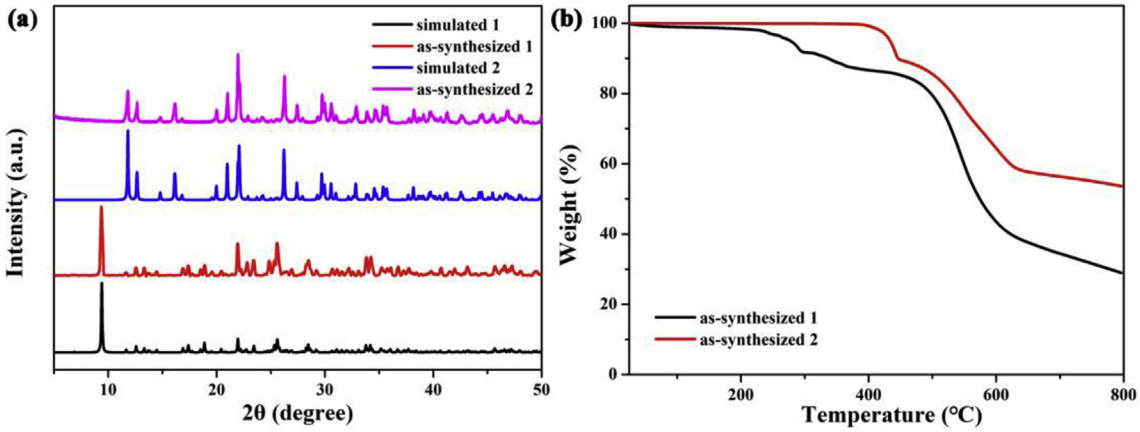


**Fig. 3.** (a) PXRD profiles of simulated and as-synthesized samples; and (b) TGA curves of fresh as-synthesized samples.

**Table 2**
Results of Knoevenagel condensation reactions based on different aldehyde reactants.

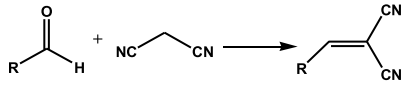

| Entry | Substrate | Product | Yield (%) |
|---|---|---|---|
| 1 |  |  | >99 |
| 2 |  | 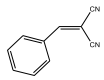 | 8 |
| 3 | 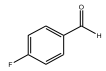 |  | >99 |
| 4 | 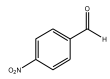 | 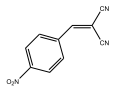 | >99 |
| 5 |  | 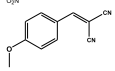 | 81 |
| 6 | 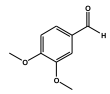 | 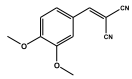 | 72 |

asymmetric unit, complex **2** owns two $Pb^{II}$ atoms, two crystallographically independent $Cl^-$ atoms, and one full deprotonated L–$O^{2-}$ bridging ligand (Fig. S2). As found in Fig. 2a, there are two significantly different $Pb^{II}$ centers in the whole structure. Pb1 is surrounded by six atoms from four oxygen-donors from one –$O^-$ and two –$COO^-$ groups, and two $Cl^-$ atoms, while Pb2 is connected by five atoms from one –$O^-$ and two –$COO^-$ groups, one nitrogen-donor from pyridine, and one $Cl^-$ bridging atom. Fig. 2b shows that only one coordination mode of the L–$O^{2-}$ bridging ligand in complex **2**, which is connected with six $Pb^{II}$ atoms by the coordination mode as $\mu_6$-$\eta^2$: $\eta^1$: $\eta^2$: $\eta^2$. As shown in Fig. 2c–e, all $Pb^{II}$ centers are linked with each other by nitrogen and oxygen-donors from the L–$O^{2-}$ bridging ligands to construct a new 3D network, which is remarkably different network with that of complex **1** due to the different organic functional groups.

### 3.2. PXRD and thermal analysis

PXRD profiles of fresh **1** and **2** were both measured in solid state at room temperature. The characteristic peaks of achieved samples are matched very well with the simulated PXRD patterns. The measurement results evidently show that as-synthesized block samples are the phase purities and same with the obtained single crystal (Fig. 3a). TGA curves of as-synthesized **1** and **2** are both shown in Fig. 3b, clearly displaying that they are able to keep their whole constructions at relative high temperature. The first weight loss of complex **1** is probably ascribed to removing guest and coordinated molecules. The second weight loss of complex **1** and the weight reduction of complex **2** are mainly attributed to structure collapse and disintegration at high temperature. The above

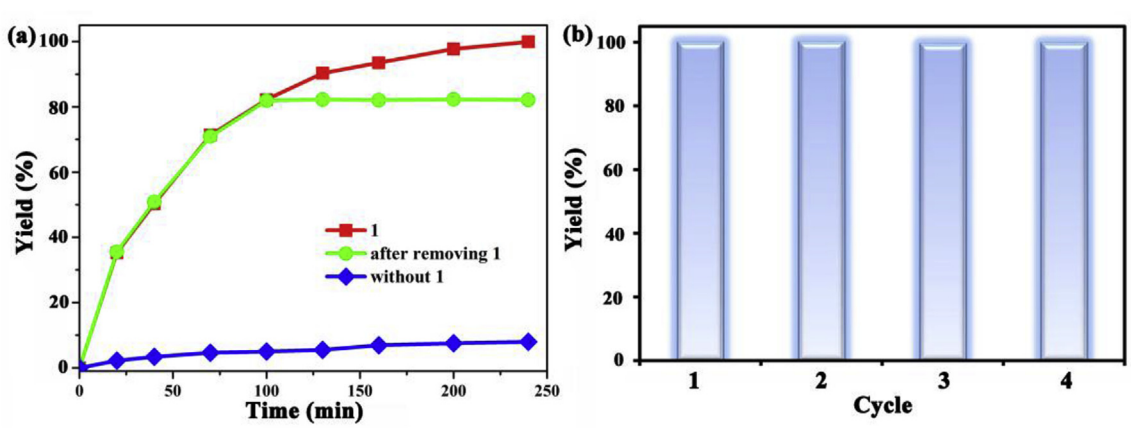


**Fig. 4.** The kinetic rate (a) and the recyclability (b) of complex **1** for this reaction.

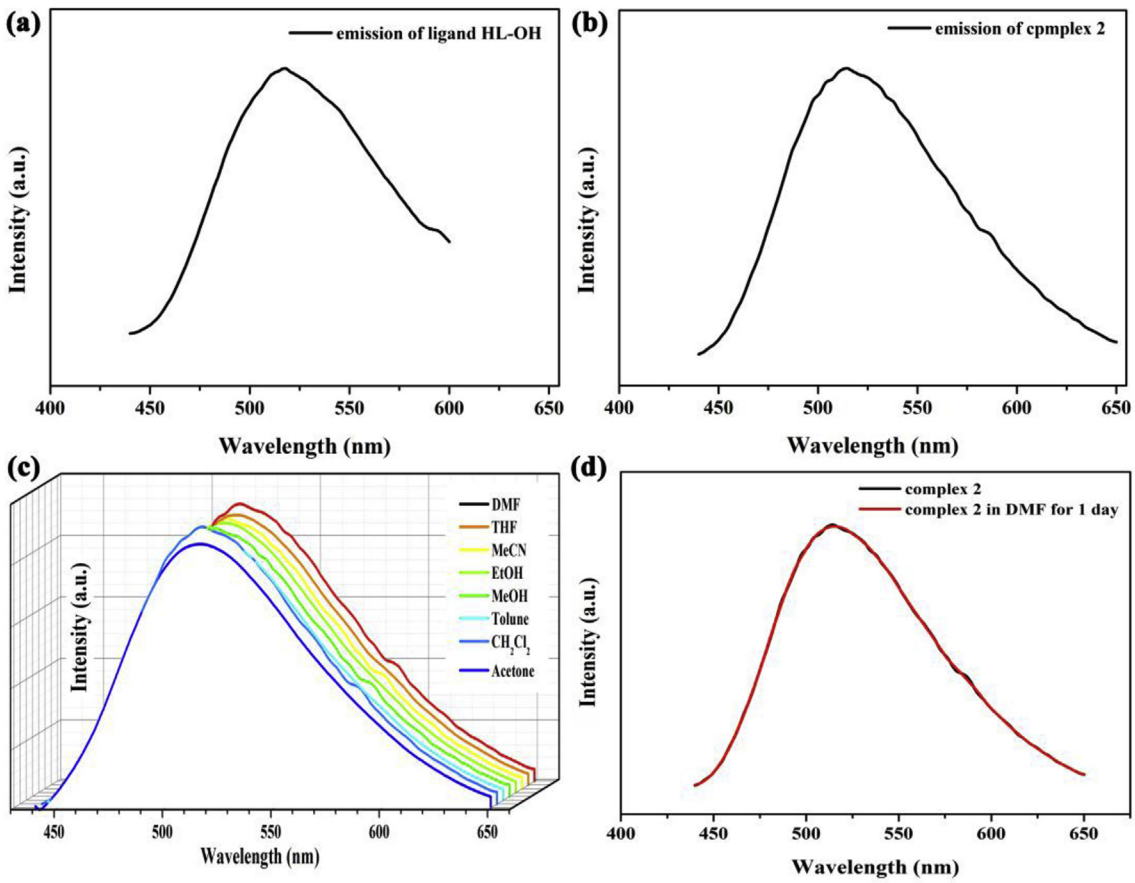


**Fig. 5.** Luminescence spectra of free HL–OH linker (a) and complex **2** (b) in solid state; (c) emission spectra of complex **2** in different organic solvents; and (d) emission intensities of ground **2** in DMF for one day.

results clearly prove that as-synthesized **1** and **2** both have relatively good thermal stabilities.

### 3.3. Catalytic properties

By virtue of Lewis base catalytic centers in complex **1** from single structure, the obtained **1** is able to investigate and consider as a catalyst for the classical Knoevenagel condensation reaction as a chemical reaction model (Table 1) [41–44]. Firstly, fresh **1** was carefully immersed in toluene overnight and then dried in air before reaction. In a representative catalytic process, the substrate of this reaction with different functional groups (1 mmol) and malononitrile (1.1 mmol) were both added in a round-bottom flask with toluene (5 mL). After complex **1** (~100 mg) was added into the above reaction system and slowly stirred at 85 °C for 5 h in an oil bath. Table 2 has all catalytic results of various substrates in this work. As illustrated in entry 1, the catalytic yield of 2-benzylidenemalononitrile product is almost 100% completely. Meanwhile, this reaction was selected and studied as an organic reaction model to explore the kinetic rates (Fig. 4a). The results clearly exhibit that this studied reaction is almost complete reaction after 5 h. To confirm the necessity of catalyst **1** for this Knoevenagel condensation reaction, the catalytic reaction is immediately terminated after dislodging catalysis **1**. The terminal catalytic yield is only 8% without **1** (entry 2). It is distinctly ensured that complex **1** is prerequisite for this reaction and plays a significant role to trigger this reaction process. In addition, aldehyde reactants with various groups are selected and used to discuss the catalytic efficiencies of complex **1** to these reactants. Entries 3 and 4 exhibit that the catalytic yields are both significantly higher than 99% because of the strong withdrawing groups of –F and $–NO_2$ in the aldehyde reactants to enhance the reaction efficiency [48–50]. However, the aldehyde reactants with large size and electron-donor –OMe group can remarkably decrease the catalytic yields to 81% and 72% for one –OMe group (entry 5) and two –OMe groups (entry 6) as substituent groups, respectively.

Reusability is also a vital element to appraise heterogeneous catalysts for real applications. Catalyst **1** is easily re-collected by fast centrifugation at 10000 $r \cdot min^{-1}$ about 2 min and further washing with fresh toluene carefully for some times. As displayed in Fig. 4b, the catalytic ability of reused complex **1** can preserve well due to its good stability. PXRD data of reused **1** after four times obviously illustrated that the framework of recycled sample can keep very well during the catalytic and recycle process (Fig. S3).

### 3.4. Luminescent sensing properties

As illustrated in Fig. 5a and b, the luminescent spectrum of isolated HL–OH ligand and prepared **2** were both discussed and measured in detail at indoor temperature. The organic linker and **2** both displayed the strongest emission peaks at 515 and 516 nm under the excitation light at 358 nm, respectively. The results illustrated that the luminescent property of complex **2** comes from HL–OH ligand and is similar with that of the free organic ligand. Taking into consider of the luminescent property of complex **2**, it encouraged us to investigate sample **2** as a sensing material to detect metal ions. As shown in Fig. 5c and d, the emission intensities of **2** are collected in different organic solvents at room temperature, including *N*, *N*-dimethylformamide (DMF), tetrahydrofuran (THF), acetonitrile (MeCN), dichloromethane ($CH_2Cl_2$), acetone, tolune, methanol (MeOH), and ethanol (EtOH); meanwhile, as-synthesized **2** can well keep its origin luminescent intensity and position in DMF for 1 day. Therefore, all detectable tests were measured and studied directly in DMF.

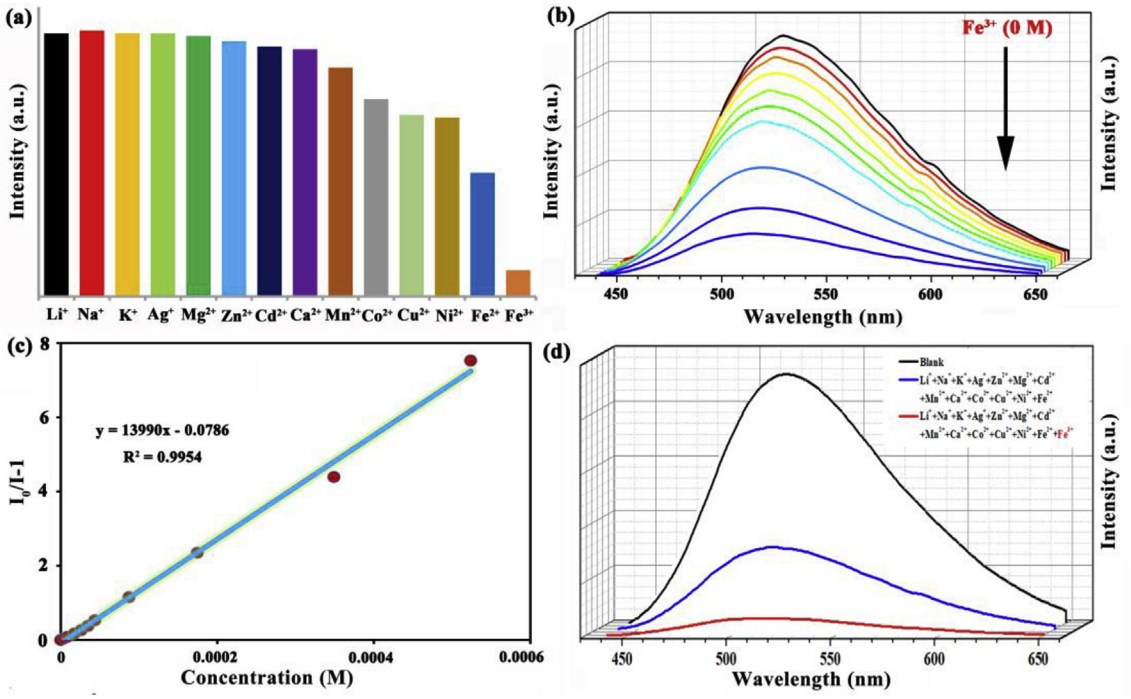


**Fig. 6.** (a) Emission spectra of complex **2** in DMF solution with different metal cations; (b) the relationship between emission intensities of **2** and $Fe^{3+}$ concentrations; (c) the Stern-Volmer plots of complex **2** for $Fe^{3+}$; and (d) the selective experiment for $Fe^{3+}$ in the present of other interfering metal cations.

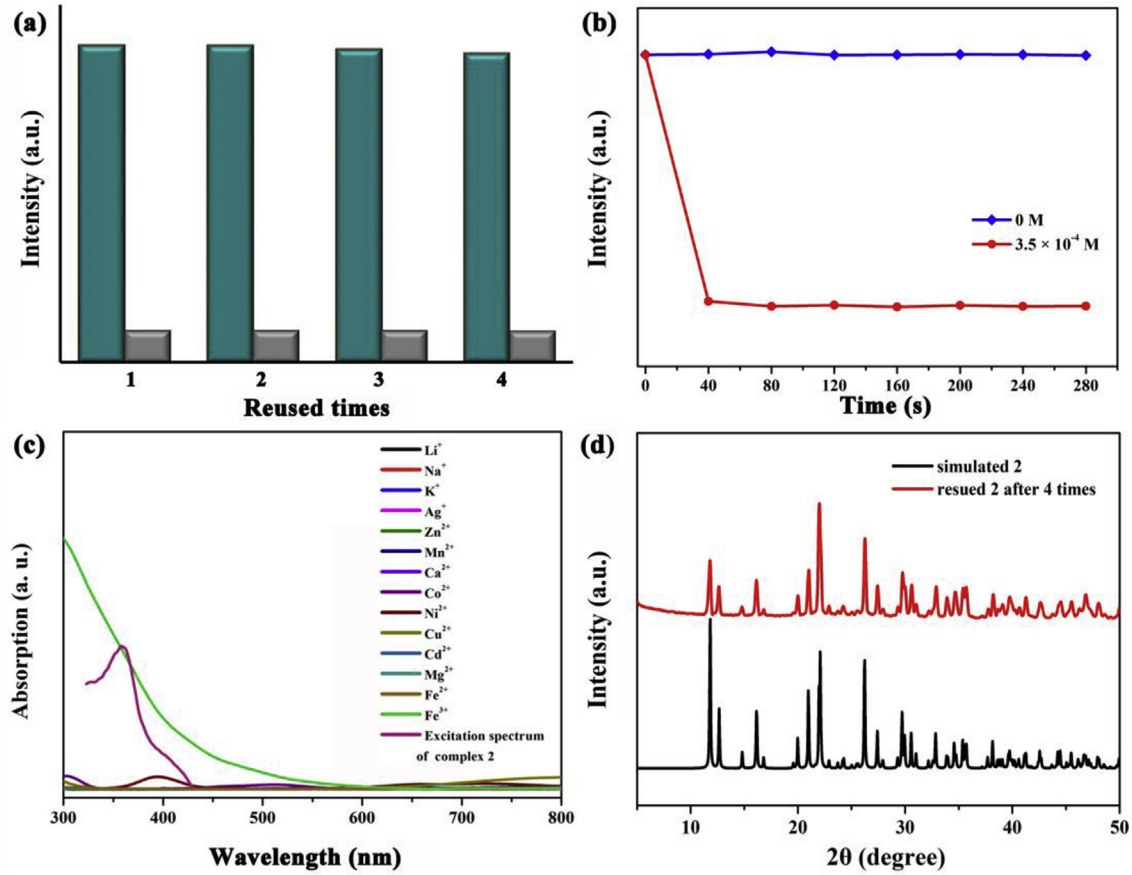


**Fig. 7.** (a) Reproducibility of ground **2** for $Fe^{3+}$ at $3.5 \times 10^{-4}$ mol $L^{-1}$; (b) luminescent response for $Fe^{3+}$ at different time intervals; (c) UV–Vis adsorption spectra of selected metal cations; and (d) the PXRD profile of ground **2** after reusing four times.

Luminescent sensing efficiencies of ground **2** were collected detaily for different metal cations. The ground **2** (3 mg) was well spread out in 3 mL of DMF solution containing $M(NO_3)_x$ ($M^{x+} = Li^+$, $Na^+$, $K^+$, $Ag^+$, $Zn^{2+}$, $Mn^{2+}$, $Mg^{2+}$, $Cd^{2+}$, $Ca^{2+}$, $Co^{2+}$, $Cu^{2+}$, $Ni^{2+}$, $Fe^{2+}$, and $Fe^{3+}$ at the concentration of $7.5 \times 10^{-4}$ mol $L^{-1}$), respectively. All luminescent data can be collected at indoor temperature after stirring slowly for 2 min. As displayed in Fig. 6a, the sensing results obviously show that a completely quenching behaviour can be detected only in the presence of $Fe^{3+}$. To well and truly appraise the sensing ability to $Fe^{3+}$, $Fe^{3+}$ titration experiments were performed and measured for ground **2** by gradually introducing $Fe^{3+}$ cation into the examination system. Fig. 6b illustrates that the luminescent intensities of ground **2** significantly decreased with the increasing concentration of $Fe^{3+}$. As we know, the Stern-Volmer constant ($K_{sv}$) is always used to appraise the detectability for complex **2** to $Fe^{3+}$. The expression of Stern-Volmer equation is $I_0/I = K_{sv}$ [Q] + 1, which I and $I_0$ are the intensities of complex **2** with and without $Fe^{3+}$; [Q] is the $Fe^{3+}$ molar concentration ($M^{-1}$). If a linear relationship between the value of ($I_0/I$) – 1 and [Q], the $K_{sv}$ value will be precisely calculated and achieved. The $K_{sv}$ value of ground **2** for $Fe^{3+}$ is $\sim 1.4 \times 10^4$ $M^{-1}$ in Fig. 6c. The detection limit of $Fe^{3+}$ can be calculated from 3δ/slope (δ: standard error) and as low as $7.61 \times 10^{-6}$ mol $L^{-1}$. The quenching efficiency of complex **1** for $Fe^{3+}$ is ~90.1% at $5.2 \times 10^{-4}$ M. More importantly, selective trials of $Fe^{3+}$ cation were investigated at room temperature with interfering caions. Fig. 6d exhibits that the emission intensity of **2** only has a little quenching behaviour, but it is almost entire quench once meeting $Fe^{3+}$ in the mixture system. The obtained results clearly illustrated that ground **2** has the excellent sensing selectivity for $Fe^{3+}$ cation by quenching response.

The reusability of ground **2** is a remarkably important factor for the sensing materials. Ground sample **2** is able to re-collect and re-generate by simple centrifugation and washing with fresh DMF several times. Fig. 7a can prove that complex **2** can keep and regenerate the luminescent detectability at least four cycles. The probable quenching mechanism was explored and analysed by some experiments. As shown in Fig. 7b, luminescent response rates of ground **2** for $Fe^{3+}$ at different time intervals obviously show that the luminescent signal can reach the terminal value very quickly and keep for a long time. It evidently shows that the quenching performance is not caused by capturing guest metal cations, which is also consistent well with the no-porous single crystal. Fig. 7c exhibits all UV–Vis absorption spectra of detectable metal cations and the excitation emission of complex **2**. It is obviously found that only $Fe^{3+}$ cation possesses a significant spectral overlap with complex **2**'s excitation peak, Hence, it can deduce that the quenching mechanism may be due to energy competitive between **2** and $Fe^{3+}$ [51–54]. The recycled PXRD profile of ground **2** after reusing four cycles exhibits that the entire skeletal framework can preserve well during all sensing experiments (Fig. 7d).

## 4. Conclusion

In conclusion, two $Pb^{II}$-based complexes were successfully designed and constructed by tuning $–NH_2$ and –OH substituting effect in the organic linkers. Complex **1** is a good heterogeneous catalyst for Knoevenagel condensation reaction. Furthermore, complex **2** can be used as a fast response and high selective sensor material for $Fe^{3+}$ in DMF solution with $K_{sv}$ value as high as $\sim 1.4 \times 10^4$ $M^{-1}$. Meanwhile, they both have excellent stability for the recyclability with the original properties. This work provides a systematic research to design and tune coordination complexes with their potential applications.

## Appendix A. Supplementary data

Supplementary data to this article can be found online at https://doi.org/10.1016/j.jssc.2019.120927.

## References


[1] L. Wang, H. Xu, J. Gao, J. Yao, Q. Zhang, Recent progress in metal-organic frameworks-based hydrogels and aerogels and their applications, Coord. Chem. Rev. 398 (2019) 213016.

[2] W. Zhou, D.-D. Huang, Y.-P. Wu, J. Zhao, T. Wu, J. Zhang, D.-S. Li, C. Sun, P. Feng, X. Bu, Stable hierarchical bimetal–organic nanostructures as highPerformance electrocatalysts for the oxygen evolution reaction, Angew. Chem. Int. Ed. 58 (2019) 4227–4231.

[3] C. Li, H. Xu, J. Gao, W. Du, L. Shangguan, X. Zhang, R.-B. Lin, H. Wu, W. Zhou, X. Liu, J. Yao, B. Chen, Tunable titanium metal–organic frameworks with infinite 1D Ti–O rods for efficient visible-light-driven photocatalytic $H_2$ evolution, J. Mater. Chem. 7 (2019) 11928–11933.

[4] J. Bitzer, W. Kleist, Synthetic strategies and structural arrangements of isoreticular mixed-component metal-organic frameworks, Chem. Eur J. 25 (2019) 1866–1882.

[5] Y.J. Cheng, R. Wang, S. Wang, X.J. Xi, L.F. Ma, S.Q. Zang, Encapsulating $[Mo_3S_{13}]^{2-}$ clusters in cationic covalent organic frameworks: enhancing stability and recyclability by converting a homogeneous photocatalyst to a heterogeneous photocatalyst, Chem. Commun. 54 (2018) 13563–13566.

[6] X.-K. Wang, J. Liu, L. Zhang, L.-Z. Dong, S.-L. Li, Y.-H. Kan, D.-S. Li, Y.-Q. Lan, Monometallic catalytic codels hosted in stable metal–organic frameworks for tunable $CO_2$ photoreduction, ACS Catal. 9 (2019) 1726–1732.

[7] Y. Zhao, D.S. Deng, L.F. Ma, B.M. Ji, L.Y. Wang, A new copper-based metal–organic framework as a promising heterogeneous catalyst for chemo-and regio-selective enamination of β-ketoesters, Chem. Commun. 49 (2013) 10299–10301.

[8] H. He, J.A. Perman, G. Zhu, S. Ma, Metal-organic frameworks for $CO_2$ chemical transformations, Small 12 (2016) 6309–6324.

[9] D. Zhang, Z.-Z. Xue, J. Pan, M.-M. Shang, Y. Mu, S.-D. Han, G.-M. Wang, Solvated lanthanide cationic template strategy for constructing iodoargentates with photoluminescence and white light emission, Cryst. Growth Des. 18 (2018) 7041–7047.

[10] W. Huang, F. Pan, Y. Liu, S. Huang, Y. Li, J. Yong, Y. Li, A.M. Kirillov, D. Wu, An efficient blue-emissive metal–organic framework (MOF) for lanthanide-encapsulated multicolor and stimuli-responsive luminescence, Inorg. Chem. 56 (2017) 6362–6370.

[11] Y. Dai, J.-J. Zhang, S.-Q. Liu, H. Zhou, Y.-J. Sun, Y.-Z. Pan, J. Ni, J.-S. Yang, A trichromatic and white-light-emitting MOF composite for multi-dimensional and multi-response ratiometric luminescent sensing, Chem. Eur J. 24 (2018) 9555–9564.

[12] Y. Zhao, X.G. Yang, X.M. Lu, C.D. Yang, N.N. Fan, Z.T. Yang, L.Y. Wang, L.F. Ma, $\{Zn_6\}$ cluster based metal–organic framework with enhanced room-temperature phosphorescence and optoelectronic performances, Inorg. Chem. 58 (2019) 6215–6221.

[13] G.-W. Xu, Y.-P. Wu, W.-W. Dong, J. Zhao, X.-Q. Wu, D.-S. Li, Q. Zhang, A multifunctional Tb-MOF for highly discriminative sensing of $Eu^{3+}/Dy^{3+}$ and as a catalyst support of Ag nanoparticles, Small 13 (2017) 1602996.

[14] Q.,-Q. Zhu, H. He, Y. Yan, J. Yuan, D.-Q. Lu, D.-Y. Zhang, F. Sun, G. Zhu, An exceptionally stable $Tb^{III}$-based metal–organic framework for selectively and sensitively detecting antibiotics in aqueous solution, Inorg. Chem. 58 (2019) 7746–7753.

[15] J. Zhao, Y.-N. Wang, W.-W. Dong, Y.-P. Wu, D.-S. Li, Q.-C. Zhang, A robust luminescent Tb(III)-MOF with Lewis basic pyridyl sites for the highly sensitive detection of metal ions and small molecules, Inorg. Chem. 55 (2016) 3265–3271.

[16] G. Zhu, M. Zhang, Y. Bu, L. Lu, X. Lou, L. Zhu, Enzyme-embedded metal-organic framework colloidosomes *via* an emulsion-based approach, Chem. Asian J. 13 (2018) 2891–2896.

[17] H.-Q. Zheng, C.-Y. Liu, X.-Y. Zeng, J. Chen, J. Lü, R.-G. Lin, R. Cao, Z.-J. Lin, J.-W. Su, MOF-808: a metal–organic framework with intrinsic peroxidase-like catalytic activity at neutral pH for colorimetric biosensing, Inorg. Chem. 57 (2018) 9096–9104.

[18] X. Lian, Y. Huang, Y. Zhu, Y. Fang, R. Zhao, E. Joseph, J. Li, J.-P. Pellois, H.-C. Zhou, Enzyme-MOF nanoreactor activates nontoxic paracetamol for cancer therapy, Angew. Chem. Int. Ed. 57 (2018) 5725–5730.

[19] H.-R. Fu, Y. Zhao, Z. Zhou, X.-G. Yang, L.-F. Ma, Neutral ligand TIPA-based two 2D metal–organic frameworks: ultrahigh selectivity of $C_2H_2/CH_4$ and efficient sensing and sorption of Cr(VI), Dalton Trans. 47 (2018) 3725–3732.

[20] Y.-W. Peng, R.-J. Wu, M. Liu, S. Yao, A.-F. Geng, Z.-M. Zhang, Nitrogen coordination to dramatically enhance the stability of In-MOF for selectively capturing $CO_2$ from a $CO_2/N_2$mixture, Cryst. Growth Des. 19 (2019) 1322–1328.

[21] Y. Han, K. Liu, M.A. Sinnwell, L. Liu, H. Huang, P.K. Thallapally, Direct observation of $Li^+$ ions trapped in a $Mg^{2+}$-templated metal–organic framework, Inorg. Chem. 58 (2019) 8922–8926.

[22] Z. Zhou, M.-L. Han, H.-R. Fu, L.-F. Ma, F. Luo, D.-S. Li, Porous Zn(II)-based metal–organic frameworks decorated with carboxylate groups exhibiting high gas adsorption and separation of organic dyes, Dalton Trans. 47 (2018) 5359–5365.

[23] P. Sikiti, C.X. Bezuidenhout, D.P. van Heerden, L.J. Barbour, Direct in situ crystallographic visualization of a dual mechanism for the uptake of $CO_2$ gas by a flexible metal–organic framework, Inorg. Chem. 58 (2019) 8257–8262.

[24] J. Gao, J. Cong, Y. Wu, L. Sun, J. Yao, B. Chen, Bimetallic hofmann-type metal–organic framework nanoparticles for efficient electrocatalysis of oxygen evolution reaction, ACS Appl. Energy Mater. 1 (2018) 5140–5144.

[25] Y.-P. Wu, W. Zhou, J. Zhao, W.-W. Dong, Y.-Q. Lan, D.-S. Li, C. Sun, X. Bu, Surfactant-assisted phase-selective synthesis of new cobalt MOFs and their efficient electrocatalytic hydrogen evolution reaction, Angew. Chem. Int. Ed. 56 (2017) 13001–13005.

[26] S.E. Springer, J.J. Mihaly, N. Amirmokhtari, A.B. Crom, M. Zeller, J.I. Feldblyum, D.T. Genna, Framework isomerism in a series of btb-containing In-derived metal–organic frameworks, Cryst. Growth Des. 19 (2019) 3124–3129.
[27] H. He, Q. Sun, W. Gao, J.A. Perman, F. Sun, G. Zhu, B. Aguila, K. Forrest, B. Space, S. Ma, A stable metal-organic framework featuring a local buffer environment for carbon dioxide fixation, Angew. Chem. Int. Ed. 57 (2018) 4657–4662.
[28] X.G. Yang, L.F. Ma, D.P. Yan, Facile synthesis of 1D organic–inorganic perovskite micro-belts with high water stability for sensing and photonic applications, Chem. Sci. 10 (2019) 14567–14572.
[29] H.D.J. Arkawazi, R. Clowes, A.I. Cooper, T. Konno, N. Kuwamura, C.M. Pask, M.J. Hardie, Complex phase behaviour and structural transformations of metal-organic frameworks with mixed rigid and flexible bridging ligands, Chem. Eur J. 25 (2019) 1353–1362.
[30] X.-X. Wu, H.-R. Fu, M.-L. Han, Z. Zhou, L.-F. Ma, Tetraphenylethyleneimmobilized metal–organic frameworks: highly sensitive fluorescent sensor for the detection of $Cr_2O_7^{2-}$ and nitroaromaticexplosives, Cryst. Growth Des. 17 (2017) 6041–6048.
[31] F. Guo, Z. Chu, M. Zhao, B. Zhu, X. Zhang, Anion-templated assembly of three metal-organic frameworks with diverse structures for highly selective detection of $Cr_2O_7^{2-}$ and $Fe^{3+}$ in aqueous solution, J. Solid State Chem. 274 (2019) 92–99.
[32] H.R. Fu, N. Wang, J.H. Qin, M.L. Han, L.F. Ma, F. Wang, Spatial confinement of a cationic MOF: a SC-|SC approach for high capacity Cr(VI)-oxyanion capture in aqueous solution, Chem. Commun. 54 (2018) 11645–11648.
[33] J. Gao, M. He, Z.Y. Lee, W. Gao, W.-W. Xiong, Y. Li, R. Ganguly, T. Wu, Q. Zhang, A surfactant-thermal method to prepare four new three-dimensional heterometal–organic frameworks, Dalton Trans. 42 (2013) 11367–11370.
[34] H. Kim, H. Kim, K. Kim, E. Lee, Structural control of metal–organic framework bearing N-heterocyclic imidazolium cation and generation of highly stable porous structure, Inorg. Chem. 58 (2019) 6619–6627.
[35] B. Dwivedi, A. Shrivastava, L. Negi, D. Das, Colossal positive and negative axial thermal expansion induced by scissor-like motion of a two-dimensional hydrogen bonded network in an organic salt, Cryst, Growth Des 19 (2019) 2519–2524.
[36] M. Sun, Q.-Q. Wang, C. Qin, C.-Y. Sun, X.-L. Wang, Z.-M. Su, An amine-functionalized zirconium metal-organic polyhedron photocatalyst with high visible-light activity for hydrogen production, Chem. Eur J. 25 (2019) 2824–2830.
[37] K. Roztocki, D. Jedrzejowski, M. Hodorowicz, I. Senkovska, S. Kaskel, D. Matoga, Effect of linker substituent on layers arrangement, stability, and sorption of Zn-isophthalate/acylhydrazone frameworks, Cryst. Growth Des. 18 (2018) 488–497.
[38] J. Zha, X. Zhang, Room-temperature synthesis of two-dimensional metal–organic frameworks with controllable size and functionality for enhanced $CO_2$ sorption, Cryst. Growth Des. 18 (2018) 3209–3214.
[39] N. Chatterjee, C.L. Oliver, A dynamic, breathing, water-Stable, partially fluorinated, two-periodic, mixed-ligand Zn(II) metal–organic framework modulated by solvent exchange showing a large change in cavity size: gas and vapor sorption studies, Cryst. Growth Des. 18 (2018) 7570–7578.
[40] Y. Wang, X. Wang, X. Wang, X. Zhang, W. Fan, D. Liu, L. Zhang, F. Dai, D. Sun, Effect of functional groups on the adsorption of light hydrocarbons in fmj-type metal–organic frameworks, Cryst. Growth Des. 19 (2019) 832–838.
[41] W. Fan, Y. Wang, Q. Zhang, A. Kirchon, Z. Xiao, L. Zhang, F. Dai, R. Wang, D. Sun, An amino-functionalized metal-organic framework, based on a rare $Ba_{12}(COO)_{18}(NO_3)_2$ cluster, for efficient $C_3/C_2/C_1$ separation and preferential catalytic performance, Chem. Eur J. 24 (2018) 2137–2143.
[42] Y. Zhang, Y. Wang, L. Liu, N. Wei, M.-L. Gao, D. Zhao, Z.-B. Han, Robust bifunctional lanthanide cluster based metal-organic frameworks (MOFs) for tandem deacetalization-Knoevenagel reaction, Inorg. Chem. 57 (2018) 2193–2198.
[43] H. Liu, F.-G. Xi, W. Sun, N.-N. Yang, E.-Q. Gao, Amino- and sulfo-bifunctionalized metal-organic frameworks: one-pot tandem catalysis and the catalytic sites, Inorg. Chem. 55 (2016) 5753–5755.
[44] W. Fan, Y. Wang, Z. Xiao, L. Zhang, Y. Gong, F. Dai, R. Wang, D. Sun, A stable amino-functionalized interpenetrated metal-organic framework exhibiting gas selectivity and pore-size-dependent catalytic performance, Inorg. Chem. 56 (2017) 13634–13637.
[45] G.M. Sheldrick, A short history of *SHELX*, ActaCryst. A 64 (2008) 112–122.
[46] G.M. Sheldrick, Crystal structure refinement with SHELXL, ActaCryst. C 71 (2015) 3–8.
[47] O.V. Dolomanov, L.J. Bourhis, R.J. Gildea, J.A.K. Howard, H. Puschmann, *OLEX2*: a complete structure solution, refinement and analysis program, J. Appl. Crystallogr. 42 (2009) 339–341.
[48] H. He, Q.-Q. Zhu, F. Sun, G. Zhu, Two 3D metal–organic frameworks based on $Co^{II}$ and $Zn^{II}$ clusters for Knoevenagel condensation reaction and highly selective luminescence sensing, Cryst. Growth Des. 18 (2018) 5573–5581.
[49] Y. Luan, Y. Qi, H. Gao, R.S. Andriamitantsoa, N. Zheng, G. Wang, A general post-synthetic modification approach of amino-tagged metal–organic frameworks to access efficient catalysts for the Knoevenagel condensation reaction, J. Mater. Chem. 3 (2015) 17320–17331.
[50] H. He, Y.-Q. Xue, S.-Q. Wang, Q.-Q. Zhu, J. Chen, C.-P. Li, M. Du, A double-walled bimetal–organic framework for antibiotics sensing and size-selective catalysis, Inorg. Chem. 57 (2018) 15062–15068.
[51] Y. Dong, H. Zhang, F. Lei, M. Liang, X. Qian, P. Shen, H. Xu, Z. Chen, J. Gao, J. Yao, Benzimidazole-functionalized Zr-UiO-66 nanocrystals for luminescent sensing of $Fe^{3+}$ in water, J. Solid State Chem. 245 (2017) 160–163.
[52] J. Wang, L. Gao, J. Zhang, L. Zhao, X. Wang, X. Niu, L. Fan, T. Hu, Syntheses, gas adsorption, and sensing properties of solvent-controlled Zn(II) pseudo-supramolecular Isomers and Pb(II) supramolecular isomers, Cryst. Growth Des. 19 (2019) 630–637.
[53] W.-H. Huang, J. Ren, Y.-H. Yang, X.-M. Li, Q. Wang, N. Jiang, J.-Q. Yu, F. Wang, J. Zhang, Water-stable metal–organic frameworks with selective sensing on $Fe^{3+}$ and nitroaromatic explosives, and stimuli-responsive luminescence on lanthanide encapsulation, Inorg. Chem. 58 (2019) 1481–1491.
[54] G.-X. Wen, Y.-P. Wu, W.-W. Dong, J. Zhao, D.-S. Li, J. Zhang, An ultrastable Europium(III)-organic framework with the capacity of discriminating $Fe^{2+}/Fe^{3+}$ ions in various solutions, Inorg. Chem. 55 (2016) 10114–10117.